HHS Public Access

Author manuscript

Nat Microbiol. Author manuscript; available in PMC 2018 May 20.

Published in final edited form as:

Nat Microbiol. 2018 February ; 3(2): 141–147. doi:10.1038/s41564-017-0060-z.

Antiviral CD8 T cells induce Zika virus associated paralysis in mice

Kellie A. Jurado[1], **Laura J. Yockey**[1], **Patrick W. Wong**[1], **Sarah Lee**[1], **Anita J. Huttner**[2], and **Akiko Iwasaki**[1,3,#]

[1]Department of Immunobiology, Yale University School of Medicine, New Haven, CT, 06520, USA

[2]Department of Pathology, Yale University School of Medicine, New Haven, CT 06520, USA

[3]Howard Hughes Medical Institute, Chevy Chase, MD, 20815,USA

Abstract

Zika virus (ZIKV) is an emerging, mosquito-borne RNA virus. The rapid spread of ZIKV within the Americas has unveiled microcephaly[1] and Guillain-Barré syndrome [2,3] as ZIKV-associated neurological complications. Recent reports have further indicated other neurological manifestations to be associated with ZIKV including myelitis [4], meningoencephalitis [5] and fatal encephalitis[6]. Here, we investigate the neuropathogenesis of ZIKV infection in IFNAR knockout (*Ifnar1*$^{-/-}$) mice, an infection model that exhibits high viral burden within the central nervous system (CNS). We show that systemic spread of ZIKV from the site of infection to the brain requires *Ifnar1*-deficiency in the hematopoietic compartment. However, spread of ZIKV within the CNS is supported by *Ifnar1*-deficient non-hematopoietic cells. Within this context, ZIKV infection of astrocytes results in breakdown of the blood-brain barrier and a large influx of CD8^{+} effector T cells. Further, we find antiviral activity of CD8^{+} T cells within the brain markedly limits ZIKV infection of neurons, but as a consequence instigates ZIKV-associated paralysis. Taken together, our study uncovers mechanisms underlying ZIKV-neuropathogenesis within a susceptible mouse model and suggests BBB breakdown and T cell mediated neuropathology as potential underpinnings of ZIKV-associated neurological complications in humans.

ZIKV inhibits type I interferon (IFN) receptor (IFNAR) signaling in human ZIKV infections, but not mice [7]. Thus, mouse models of ZIKV infection necessitate use of genetic deficiencies in IFNAR or antibody blockade of IFNAR [8–10]. To examine immune responses

[#]Correspondence: Akiko Iwasaki, Department of Immunobiology, Yale University School of Medicine, The Anlyan Center for Medical Research and Education, 300 Cedar Street, New Haven, CT 06520. Phone: (203) 785-2919 akiko.iwasaki@yale.edu. Correspondence and requests for materials should be addressed to A.I. (akiko.iwasaki@yale.edu).

We declare no competing financial interests.

Competing interests. The authors declare no competing financial interests.

Author contributions

K.A.J. and A.I. planned the project, designed experiments, analyzed and interpreted data and wrote the manuscript. K.A.J., P.W.W, S.L. and L.Y. designed and performed experiments. A.H. assisted in histopathological analysis.

Data availability. The data that support the findings of this study are available from the corresponding author upon request.

that control ZIKV neuropathogenesis, we first probed the cellular compartment responsible for the type I IFN-dependent block of ZIKV infection using irradiation-induced bone marrow chimeric mice between ZIKV-resistant C57BL/6 CD45.1 (WT) and ZIKV-susceptible interferon α/β receptor-deficient (*Ifnar1*$^{-/-}$) mice. This approach allowed us to differentiate type I IFN-dependency of brain non-hematopoietic cells (i.e. endothelial, astrocyte or neuron) versus hematopoietic cells (i.e. lymphocytes or leukocyte) in mediating ZIKV spread and neuropathology. *Ifnar1*$^{-/-}$ mice reconstituted with *Ifnar1*$^{-/-}$ bone marrow (*Ifnar1*$^{-/-}$ → Ifnar1$^{-/-}$) were the only chimeric combination to lose weight (Figure 1a) and present with the symptoms of hindlimb paralysis (Figure 1b). WT mice reconstituted with *Ifnar1*$^{-/-}$ bone marrow (*Ifnar1*$^{-/-}$ → WT) had significantly levels of viremia (Figure 1c), but had very low brain viral load (Figure 1d). It is possible that the lower rates of infection in the brain within *Ifnar1*$^{-/-}$ → WT mice could be due to lower levels of virus within the blood. Additionally, the low levels of ZIKV RNA detected within the brain of the other chimeras may be representative of virus within residual blood. Nevertheless, these data indicated that, while systemic spread of ZIKV requires *Ifnar1*-deficiency within the hematopoietic compartment, *Ifnar1*-deficiency within hematopoietic cells is not sufficient to cause neurological viral amplification and disease.

Our data are consistent with recent work showing viremia, but limited brain infection and lack of neuropathology in LysMCre^{+}*Ifnar1*$^{fl/fl}$ mice[11]. Moreover, our data indicate that *Ifnar1*-dependent block of ZIKV within brain non-hematopoietic cells controls the viral replication and associated neurological disease manifestation of a ZIKV infection. To identify the cell types that support ZIKV replication in the CNS, we conducted immunofluorescence staining of ZIKV-infected adult *Ifnar1*$^{-/-}$ brains 7 days post infection (DPI), a time when the majority of infected mice present with neurological complications and a high viral load is measured. Despite multiple cell types evaluated (microglia and oligodendrocytes (Supplemental Figure 1a and 1b)), we found that ZIKV infection is largely confined to astrocytes and to a lesser extent, within neurons of the cerebral cortex (Figure 2a). This tropism was evident in various regions within the CNS including the cerebellum, brain stem and spinal cord (Supplemental Figure 2). Despite a large number of inflammatory cells within the meninges, we did not find many positive ZIKV cells within this region 7 DPI (Supplemental Figure 1c).

Astrocytes extend their end foot processes to provide integral support for the blood brain barrier (BBB)[12]. Indeed, we observed prominent infection of the astrocyte end feet surrounding blood vessels in the CNS (Figure 2b). We predicted that ZIKV infection of astrocytes might lead to increased vascular permeability. To probe BBB breakdown, we stained for the presence of mouse IgG, which is normally blocked from accessing the CNS parenchyma by the BBB. We found bright IgG staining within infected brains of *Ifnar1*$^{-/-}$ mice, but not the *Ifnar1*-competent, wildtype ZIKV infected mice or the mock-infected *Ifnar1*$^{-/-}$ controls (Figure 2c). Consistently, intravenous injection of fluorescently-labeled dextran at the peak of ZIKV-disease presentation provided functional demonstration of a ZIKV-induced BBB disruption (Figure 2d, quantified in Supplemental Figure 3c). Further, areas where increased vascular permeability was detected (by evidence of leaky dextran) corresponded to regions where astrocyte foot process lining was fragmented (Supplemental Figure 3). Analysis of the brain sections of bone marrow chimeric mice corroborated stromal

dependence in eliciting BBB breakdown, as *Ifnar1*$^{-/-}$ → *Ifnar1*$^{-/-}$ bone marrow chimeric mice were the only combination to exhibit positive IgG staining within the brain (Supplemental Figure 4). Our data therefore suggest that type I IFN signaling within astrocytes block their infection by ZIKV and prevent BBB breakdown. The neuroprotective role of the type I IFN cascade within astrocytes has recently been ascribed during the infection of another flavivirus, West Nile virus [13]. Astrocyte-specific Ifnar1-dependence for BBB leakage in ZIKV infection should be examined in future studies.

Histological analysis of ZIKV-infected *Ifnar1*$^{-/-}$ brains as compared to *Ifnar1*-competent, wildtype infected and mock, uninfected *Ifnar1*$^{-/-}$ mice indicated a vast infiltration of leukocytes on 7 DPI (Figure 3a), which were CD45^{+} (Figure 3b). Flow cytometry analysis of single-cell suspensions of infected and mock *Ifnar1*$^{-/-}$ brains further confirmed a significant increase in CD45^{+} cells 7 DPI when compared to both mock, uninfected, but also within ZIKV-infected brains 5 DPI (Figure 3c). Notably, the population of infiltrating immune cells largely comprised of T cells (CD3^{+}) at 7 DPI, which only served as a minority population at 5 DPI (Figure 3d). Further analysis indicated that the majority of CD3^{+} cells were CD8^{+} effector T cells as analyzed by flow cytometry (Figure 3e) and immunofluorescence staining revealed that many of these cells are perforin-positive (Figure 3f). This result is consistent with a previous work showing CD8^{+} T cell infiltration within the brains of ZIKV-infected immune competent neonate C57Bl/6 mice without *Ifnar1* manipulation [14]. Since we find the vast infiltration of effector T cells to coincide with CNS pathogenesis, our data suggested that either the effector T cells are reaching the brain too late to control virus replication or that their antiviral actions may be immunopathogenic.

In order to understand the effects of T cell infiltration on viral load and neuropathology of a ZIKV infection, we depleted T cells with antibodies. Notably, depletion of CD8^{+} T cells, but not CD4^{+} T cells, resulted in a significant increase in survival (Figure 4a). Yet, viral load at 7 DPI indicated a significantly higher viral load in the brain of the CD8^{+} T cell-depleted animals as compared to those intact in CD8^{+} T cells (Figure 4d). The higher viral load in CD8 T-depleted mice at 7 DPI was corroborated by ZIKV immunofluorescence within CD8^{+} T cell intact vs. depleted brain tissues (Figure 4f). These data are consistent with recent studies demonstrating elevated ZIKV replication in CD8-depleted or CD8-knockout anti-*Ifnar1* treated animals [11] or in Rag1$^{-/-}$ mice [15]. In contrast, hindlimb paralysis was strikingly abrogated in CD8-depleted mice (Figure 4b), which were euthanized due to weight loss greater than 20% rather than onset of paralysis as was the case within the undepleted or CD4-depeleted mice (Figure 4c and Supplemental Figure 5). The CD8-depleted mice had, in addition to significant weight loss, symptoms of illness including ruffled fur, hunched backs and/or tremors late in infection.

Dual depletion of CD4^{+} and CD8^{+} T cells resulted in an intermediate phenotype with a significant increase in survival, but not to the same extent as seen within solely CD8 T-depleted mice. Consistent with the intermediate increase in survival, only 1 of the 8 dual-depleted mice developed hindlimb paralysis. Interestingly, all CD4-depleted mice developed hindlimb paralysis, suggestive of a potential regulatory role of CD4^{+} T cells. Within this vein, we probed for the presence of Foxp3+ regulatory T cells within the CNS. Increased number of Foxp3+ regulatory T cells were found within ZIKV-infected animals compared to

mock-infected *Ifnar1*$^{-/-}$ mice within the brain, while comparable levels of Tregs were found in the spleen (Figure 4e). These data suggested that while CD8 T cells cause neuropathology, the CD4+ Tregs dampen the immunopathology caused by CD8 T cells.

We further investigated ZIKV-infected cell types within the brain and found that the percentage of ZIKV-positive neurons increased drastically within the CD8-depleted animals as compared to the CD8^{+} T cell intact mice at 7 DPI (Figure 4e). This difference was determined to be quantitatively significant in both the cerebral cortex and the distal spinal cord (Figure 4g). Further we found positive activated caspase 3 staining within the NeuN+ neurons with fragmented nucleus (per DAPI staining) in the ZIKV-infected brains and spinal cords 7 DPI within CD8 T cell intact mice (Supplementary Figure 6b and c, respectively, white arrow). Some of the dying neurons expressed low levels of NeuN (Supplementary Figure 6b, inset, yellow arrow). We also observed activate caspase 3 staining in rare non-neuronal cells (Supplementary Figure 6b and c, grey arrow). In contrast, activated caspase 3 staining was completely absent in the CNS of the CD8-depleted mice at 7 DPI (Supplementary Figure 6a). Lastly, we were able to visualize an immunological synapse of cytolytic cells (perforin positive) with neurons within the brain of ZIKV-infected mice (Supplemental Figure 6d). These data reveal that CD8^{+} T cell-mediated lysis of ZIKV-infected neurons, while controlling the viral load, leads to hindlimb paralysis.

In summary, our study in *Ifnar1*$^{-/-}$ deficient mice demonstrates that ZIKV infects circulating leukocytes in order to become blood borne. Once in circulation, ZIKV-infected, bone marrow derived cells facilitate viral spread to various tissues and assume organ-specific virus replication. Within the CNS, *Ifnar1*-signaling within brain non-hematopoietic cells is able to block ZIKV spread. In the absence of *Ifnar1*, astrocytes become infected with ZIKV, resulting in a loss of the BBB. BBB breakdown is accompanied by a large influx of infiltrating cells into the CNS. In particular, CD8^{+} T cells infiltrate into the brain and are able to limit ZIKV replication within neurons. However, this antiviral process comes at the cost of neuropathogenesis leading to hindlimb paralysis.

ZIKV infection of the *Ifnar1*-deficent mouse allows us to model ZIKV pathogenesis under circumstance of high viral burden within the CNS, where innate resistance is inefficient or impaired. Such conditions might mimic the settings of neonates[16], elderly[17], and immunosuppressed individuals, where innate resistance is suboptimal resulting in overdrive of compensatory immune effector mechanisms. Consistent with previous work[11,15], our findings indicate an antiviral role for CD8 T cells in the ZIKV infection. Yet under conditions of high viral burden within the CNS through use of the *Ifnar1*$^{-/-}$ mouse model, this protection resulted in lethal immunopathology. A recent postmortem analysis of human neonates with congenitally acquired ZIKV found leukocyte aggregation near blood vessels or perivascular cuffing, as a common phenotype within the brains analyzed[18]. Our data are strikingly similar in that we observed perivascular infiltration of T cells within the brains of the *Ifnar1*-deficent mice (Figure 2A). Additionally, “red neurons”, a pathological finding of apoptotic neurons within histology slides, were found within congenitally infected neonatal brains indicative of neuronal apoptosis/necrosis[18], a phenotype found within the *Ifnar1*$^{-/-}$ mice (Supplemental Figure 6). Lastly, work with primary developing human brain tissue, found ZIKV to target astrocytes for viral replication[19], also consistent with our work, these

pathology similarities suggest ZIKV infection of the *Ifnar1*-deficent mouse may serve to model some aspects of congenitally acquired ZIKV infection. However, whether CD8 T cells play a role in neonatal brain immunopathology following congenital ZIKV infection remains to be determined.

Our results suggest a potential involvement of adaptive immune response as a basis for apoptosis of infected neurons, leading to immunopathology in the setting of impaired innate resistance. Our data thereby provide a compelling basis to investigate the role of T cells and BBB breakdown within ZIKV-induced neurological complications that follow ZIKV infection in humans [20].

Methods

Mice

Ifnar$^{-/-}$ mice (# 32045-JAX) and CD45.1 mice (stock # 002014) were purchased from The Jackson Laboratory and C57BL/6 mice (strain code #027) from Charles River. Ifnar$^{-/-}$ and C57BL/6 mice were subsequently bred and housed at Yale University. Mice of both sexes were between 6–8 weeks of age for the initiation of all experiments conducted. No randomization protocol or blinding was used. Sample size was designed to provide statistical significance with a strict minimum of 3 mice per condition. All animal procedures were completed in compliance with approved Yale Institutional Animal Care and Use Committee protocols.

Virus and cells

ZIKV Cambodian FSS13025 strain (World Reference Center for Emerging Viruses and Arboviruses at University of Texas Medical Branch, Galveston) was used for all experiments. ZIKV stocks were grown in C636 cells and titered by plaque assay within Vero cells (ATCC CCL-81) as previously described [21]. C6/36 mosquito cells (*Aedes albopictus*) (ATCC CRL-1660) were maintained in Dulbecco's Modified Eagle's Medium (GIBCO) supplemented with 10% heat-inactivated fetal bovine serum, 1% penicillin/streptomycin (GIBCO) and 1% tryptose phosphate broth (Sigma) at 30 °C. Vero cells were maintained at 37 °C in Dulbecco's Modified Eagle's Medium (GIBCO) supplemented with 10% heat-inactivated fetal bovine serum, 1% penicillin/streptomycin (GIBCO). Cell lines were authenticated by morphology and are routinely tested for mycoplasma contamination.

In vivo experiments

Mice were infected with 10^6 PFU ZIKV via intra footpad injection. For bone marrow chimera studies, mice were irradiated at two doses of 475 cGy (total 950 cGy) and reconstituted with 1×10^6 WT or Ifnar1$^{-/-}$ bone marrow cells. The mice were used for experiments eight weeks after bone marrow transplantation. Chimeras were checked for efficiency of reconstitution through use of congenic bone marrow transfer. Reconstitution was determined to be 91–93% efficient in the *Ifnar1*$^{-/-}$ → WT mice, while it was 93–95% efficient within the WT → *Ifnar1*$^{-/-}$ mice. For BBB breakdown assay, at 7 DPI with ZIKV or PBS (mock), Oregon green 488-conjugated dextran (70 kDa) (5 mg ml-1, 200 μl per mouse) was injected intravenously. Forty-five minutes later, these mice were sacrificed for

immunohistochemical analysis. For depletion studies, Ifnar$^{-/-}$ mice were injected intravenously with 300 ug of anti-CD4 (GK1.5;BioXCell) and/or anti-CD8 (YPT; BioXCell) antibody at days −1, 4, 9 post ZIKV infection. Depleted mice demonstrated 90–95% efficiency of depletion treatment on day 7 post ZIKV infection. All antibodies for depletion studies were purchased from BioXCell. Mice monitored for clinical illness and were euthanized before reaching the moribund state (onset of hindlimb paralysis (the inability to move hind legs) and/or >20% weight loss) due to humane concerns.

Virus quantification

To determine ZIKV viremia, 50–100ul of blood was collected via retro-orbital bleed at indicated time points post-infection. Total RNA was extracted using Trizol (Thermo Fischer Scientific) extraction followed by purification with RNeasy Mini Kit (QIAGEN). To determine levels of virus in tissues, mice were euthanized and indicated tissues were collected and extracted in Trizol. cDNA was synthesized using iScript cDNA synthesis kit (Bio-Rad) with quantitative PCR being performed using SYBR-Green (Bio-Rad) or PrimeTime master mix (Integrated DNA Technologies) on a CFX Connect instrument (Bio-Rad). ZIKV RNA was detected using primers designed to NS5 [21], with limit of detection determined as previously described [21].

Immunofluorescence

Harvested organs were fixed in 4% paraformaldehyde (PFA) for 24 hours or IHC zinc fixative (BD Pharmingen) for anti-perforin stained tissues. Fixed tissues were then sucrose sedimented in 10%, 20% and 30% steps prior to embedding within optimum cutting temperature (O.C.T.) medium (Tissue Tek). Frozen sections of 5–7 μm thicknesses were cut and left to dry at ambient temperature. These tissues were then stained with primary antibodies: Cleaved Caspase 3 (Cell Signaling Technology), CD31 (Novus Biologicals INC), CD45 (Novus Biologicals INC), glial fibrillary acidic protein (GFAP) (Agilent Technologies INC), rabbit-neuronal marker (NeuN) (Cell Signaling Technology), guinea pig-NeuN (EMD Millipore Corporation), rat anti-perforin (Novus Biologicals INC) and anti-ZIKV rat serum [22] after rehydration with PBS (2X for 10 minutes) and permeabilization with PBST (3X for 10 minutes) at RT overnight. Slides were washed and incubated with appropriate secondary prior to a final wash series and incubation with 4′,6-diamidino-2-phenylindole (DAPI) prior to mounting with SlowFade Diamond Antifade (Fisher Scientific Company LLC). Stained tissues were then analyzed by fluorescence microscopy (BX51; Olympus) or confocal microscopy (TCS SP2; Leica).

Flow Cytometry

Preparation of single-cell suspensions from brain tissues was completed as previously described [23] using the following e-Bioscience or Biolegend antibodies: CD45.2 (104 and 30-F11), CD45.1 (A20), CD4 (RM4-5 and GK1.5), CD8 (53-6.7), CD3 (145-2C11 and 17A2), F4/80 (BM8), CD25 (PC61), GITR (DTA-1), CD127 (A7R34), FoxP3 (FJK-165), and isotype (eBRG1). Aqua Live/dead stain (ThermoFisher) and FoxP3 intracellular staining kit (eBioscience) were utilized. Multiparameter analyses were performed on an LSR II flow cytometer (BD Biosciences) and analyzed using FlowJo software (Tree Star).

Statistical Analysis

Survival curves were analyzed using a log-rank test. Variable comparisons were completed using a two-tailed unpaired Student's t-test within GraphPad Prism. We used a minimum of 3 animals per condition within any experiment. Data is represented as individual data points ± SD or ± SEM if greater than 7 data points, as stated in figure legends.

Supplementary Material

Refer to Web version on PubMed Central for supplementary material.

Acknowledgments

We thank A.N. van den Pol for providing anti-ZIKV rat serum, H. Dong and Y. Kumamoto for animal care and technical assistance, respectively. This study was in part supported by the National Institutes of Health (1R21AI131284 to A.I., T32GM007205 to L.J.Y. and 4T32AI007019-41 to K.A.J). A.I. is an investigator of the Howard Hughes Medical Institute. K.A.J. is a recipient of the Burroughs Wellcome Postdoctoral Enrichment Program.

References

1. Rasmussen SA, Jamieson DJ, Honein MA, Petersen LR. Zika Virus and Birth Defects--Reviewing the Evidence for Causality. The New England journal of medicine. 2016; 374:1981–1987. DOI: 10.1056/NEJMsr1604338 [PubMed: 27074377]
2. Cao-Lormeau VM, et al. Guillain-Barre Syndrome outbreak associated with Zika virus infection in French Polynesia: a case-control study. Lancet. 2016; 387:1531–1539. DOI: 10.1016/S0140-6736(16)00562-6 [PubMed: 26948433]
3. Oehler E, et al. Zika virus infection complicated by Guillain-Barre syndrome--case report, French Polynesia, December 2013. Euro surveillance : bulletin Europeen sur les maladies transmissibles = European communicable disease bulletin. 2014; 19
4. Mecharles S, et al. Acute myelitis due to Zika virus infection. Lancet. 2016; 387:1481. [PubMed: 26946926]
5. Carteaux G, et al. Zika Virus Associated with Meningoencephalitis. The New England journal of medicine. 2016; 374:1595–1596. DOI: 10.1056/NEJMc1602964 [PubMed: 26958738]
6. Soares CN, et al. Fatal encephalitis associated with Zika virus infection in an adult. Journal of clinical virology : the official publication of the Pan American Society for Clinical Virology. 2016; 83:63–65. DOI: 10.1016/j.jcv.2016.08.297 [PubMed: 27598870]
7. Grant A, et al. Zika Virus Targets Human STAT2 to Inhibit Type I Interferon Signaling. Cell host & microbe. 2016; 19:882–890. DOI: 10.1016/j.chom.2016.05.009 [PubMed: 27212660]
8. Lazear HM, et al. A Mouse Model of Zika Virus Pathogenesis. Cell host & microbe. 2016; 19:720–730. DOI: 10.1016/j.chom.2016.03.010 [PubMed: 27066744]
9. Dowall SD, et al. A Susceptible Mouse Model for Zika Virus Infection. PLoS neglected tropical diseases. 2016; 10:e0004658. [PubMed: 27149521]
10. Rossi SL, et al. Characterization of a Novel Murine Model to Study Zika Virus. The American journal of tropical medicine and hygiene. 2016; 94:1362–1369. DOI: 10.4269/ajtmh.16-0111 [PubMed: 27022155]
11. Elong Ngono A, et al. Mapping and Role of the CD8+ T Cell Response During Primary Zika Virus Infection in Mice. Cell host & microbe. 2017; 21:35–46. DOI: 10.1016/j.chom.2016.12.010 [PubMed: 28081442]
12. Iwasaki A. Immune Regulation of Antibody Access to Neuronal Tissues. Trends in molecular medicine. 2017; 23:227–245. DOI: 10.1016/j.molmed.2017.01.004 [PubMed: 28185790]
13. Daniels BP, et al. Regional astrocyte IFN signaling restricts pathogenesis during neurotropic viral infection. The Journal of clinical investigation. 2017; 127:843–856. DOI: 10.1172/JCI88720 [PubMed: 28134626]

14. Manangeeswaran M, Ireland DD, Verthelyi D. Zika (PRVABC59) Infection Is Associated with T cell Infiltration and Neurodegeneration in CNS of Immunocompetent Neonatal C57Bl/6 Mice. PLoS pathogens. 2016; 12:e1006004. [PubMed: 27855206]

15. Winkler CW, et al. Adaptive Immune Responses to Zika Virus Are Important for Controlling Virus Infection and Preventing Infection in Brain and Testes. Journal of immunology. 2017; 198:3526–3535. DOI: 10.4049/jimmunol.1601949

16. Cormier SA, et al. Limited type I interferons and plasmacytoid dendritic cells during neonatal respiratory syncytial virus infection permit immunopathogenesis upon reinfection. Journal of virology. 2014; 88:9350–9360. DOI: 10.1128/JVI.00818-14 [PubMed: 24920801]

17. Shaw AC, Goldstein DR, Montgomery RR. Age-dependent dysregulation of innate immunity. Nature reviews. Immunology. 2013; 13:875–887. DOI: 10.1038/nri3547

18. Sousa AQ, et al. Postmortem Findings for 7 Neonates with Congenital Zika Virus Infection. Emerging infectious diseases. 2017; 23:1164–1167. DOI: 10.3201/eid2307.162019 [PubMed: 28459414]

19. Retallack H, et al. Zika virus cell tropism in the developing human brain and inhibition by azithromycin. Proceedings of the National Academy of Sciences of the United States of America. 2016; 113:14408–14413. DOI: 10.1073/pnas.1618029113 [PubMed: 27911847]

20. Dirlikov E, et al. Guillain-Barre Syndrome During Ongoing Zika Virus Transmission - Puerto Rico, January 1–July 31, 2016. MMWR. Morbidity and mortality weekly report. 2016; 65:910–914. DOI: 10.15585/mmwr.mm6534e1 [PubMed: 27584942]

21. Yockey LJ, et al. Vaginal Exposure to Zika Virus during Pregnancy Leads to Fetal Brain Infection. Cell. 2016; 166:1247–1256e1244. DOI: 10.1016/j.cell.2016.08.004 [PubMed: 27565347]

22. van den Pol AN, Mao G, Yang Y, Ornaghi S, Davis JN. Zika Virus Targeting in the Developing Brain. The Journal of neuroscience : the official journal of the Society for Neuroscience. 2017; 37:2161–2175. DOI: 10.1523/JNEUROSCI.3124-16.2017 [PubMed: 28123079]

23. Iijima N, Iwasaki A. Access of protective antiviral antibody to neuronal tissues requires CD4 T-cell help. Nature. 2016; 533:552–556. DOI: 10.1038/nature17979 [PubMed: 27225131]

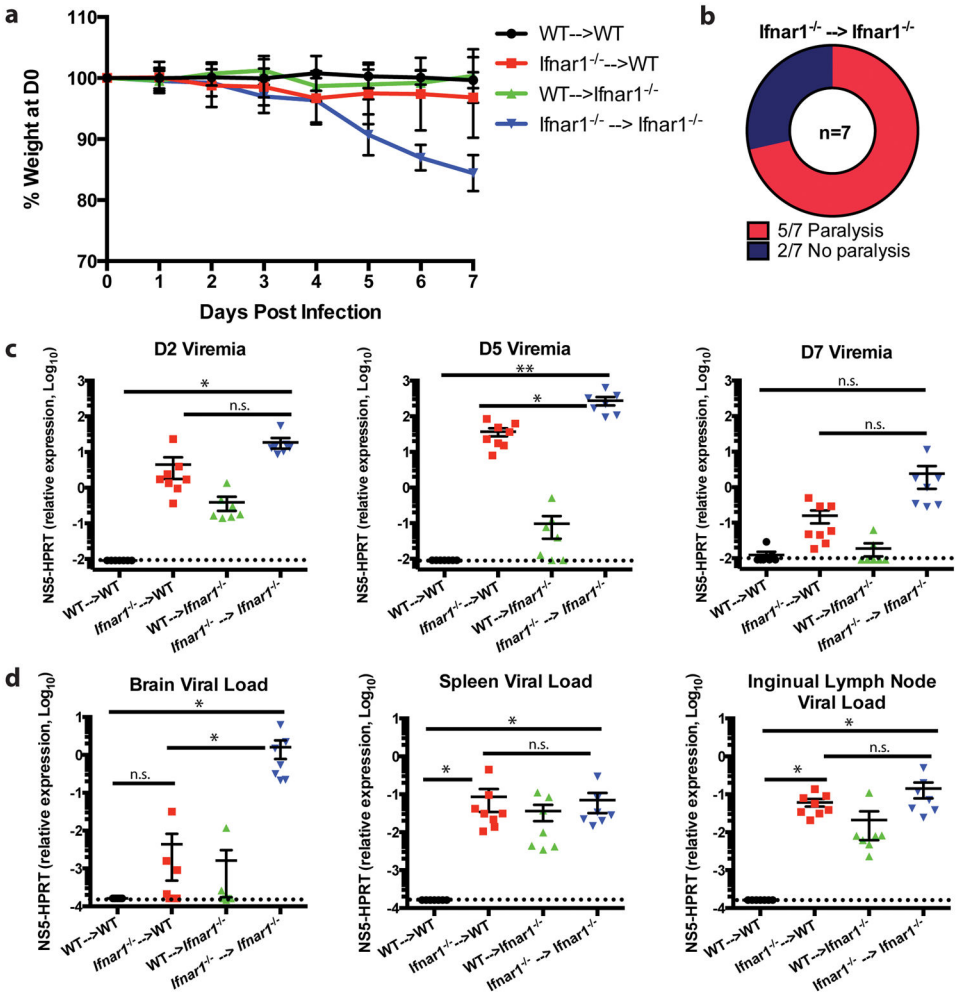

Figure 1. Systemic spread of ZIKV is dependent upon Ifnar1$^{-/-}$ deficiency in the hematopoietic compartment

a–d, *Ifnar1*$^{-/-}$ and CD45.1 C57BL/6 WT bone marrow chimeric mice (n=7 or 8 per group in two separate experiments) were infected with 10^6 plaque-forming units (p.f.u.) of ZIKV intra-footpad. Daily weight (**a**), development of hindlimb paralysis (**b**) and viremia on days 2, 5 and 7-post infection (**c**) were monitored. **d**, Seven days post infection, viral load in tissue homogenates including the brain, spleen and inguinal lymph node was measured. Data are presented as mean ± s.e.m. *P < 0.05; **P < 0.01 (two-tailed unpaired Student's t-test).

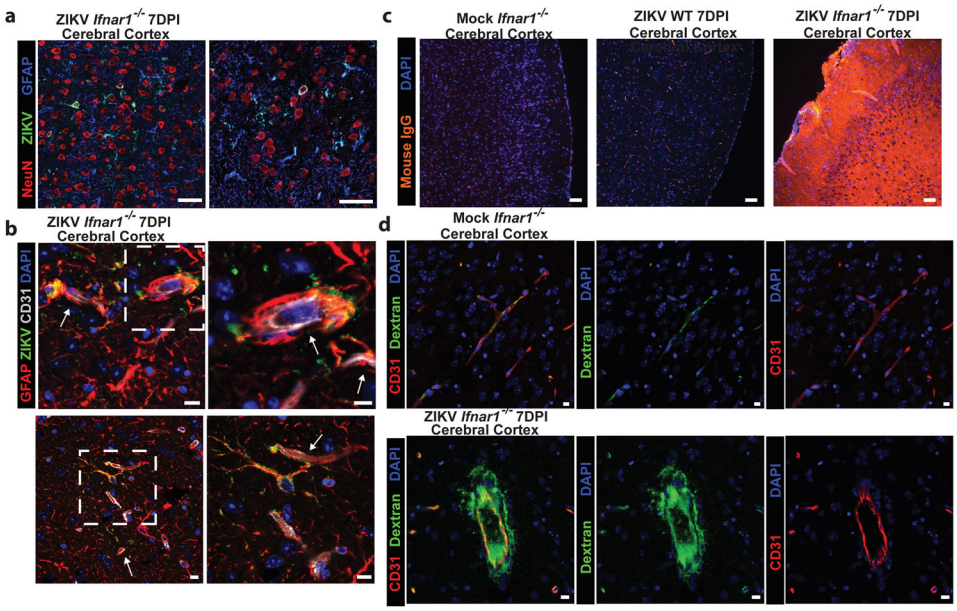

Figure 2. ZIKV infection of astrocytes is associated with breakdown of the blood-brain barrier

a–d, *Ifnar1*$^{-/-}$ (n=5) and WT (n=3) mice were infected with 10^6 plaque-forming units (p.f.u.) of ZIKV or PBS (mock) (n=4) intra-footpad in two separate experiments. Frozen sections of the brain, specifically the cerebral cortex, were stained with antibodies against astrocytes (GFAP), neurons (NeuN) and ZIKV (scale bars, 50 μm) (**a**). Brain sections, specifically the cerebral cortex, were further stained with IgG (scale bars, 100 μm) (**b**), GFAP, ZIKV, CD31 (scale bars, 10 μm with 7.5 μm inset) (**c**). White arrows indicate blood vessels surrounded by ZIKV-infected astrocytes. **d**, Seven days post infection with ZIKV or PBS (mock), Oregon green 488-conjugated dextran (70 kDa) (5 mg ml^{-1}, 200 μl per mouse) was injected intravenously in two separate experiments. Forty-five minutes later, these mice were sacrificed for immunohistochemical analysis (n=4 per infection condition). Nuclei are depicted by 4′,6-diamidino-2-phenylindole (DAPI) stain (blue) (scale bars, 10 μm).

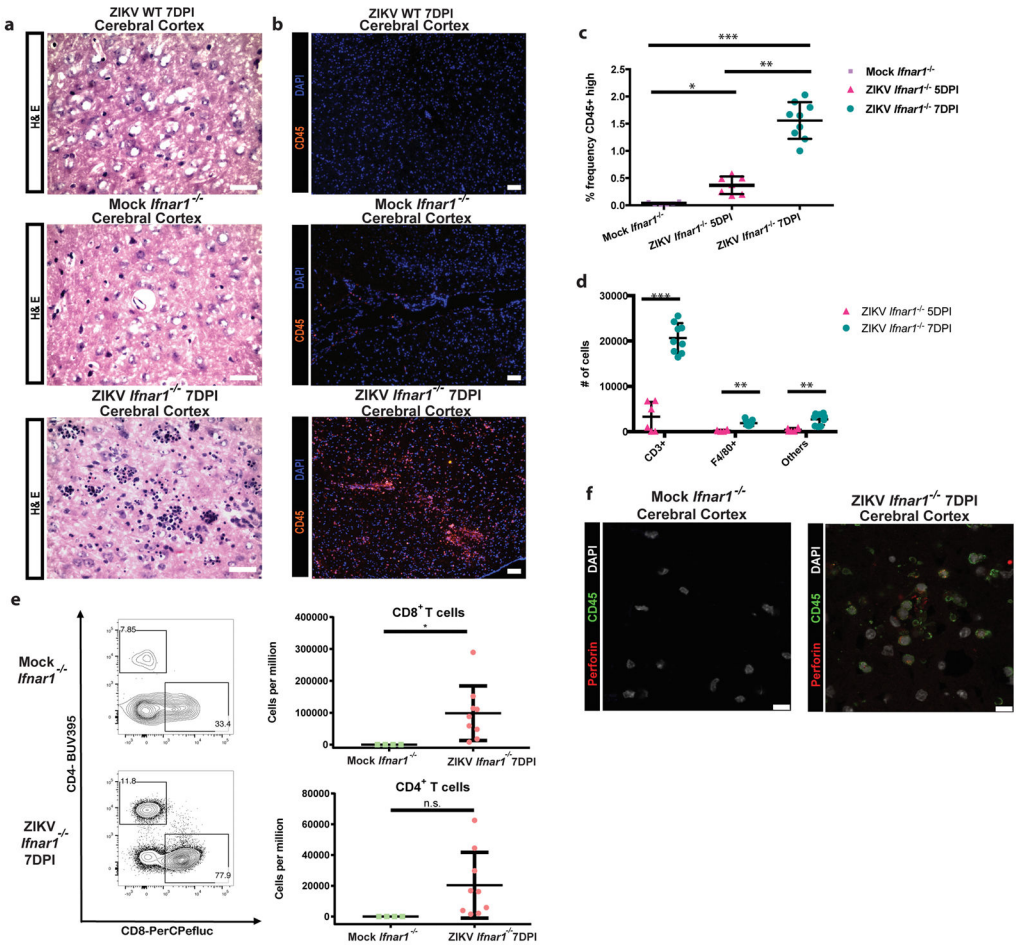

Figure 3. ZIKV replication within the brain causes a large influx of CD8$^+$ effector T cells

a–f, *Ifnar1*$^{-/-}$ (n=5) and WT (n=3) mice were infected with 10^6 plaque-forming units (p.f.u.) of ZIKV or PBS (mock) (n=4) intra-footpad in two separate experiments. Seven days post infection frozen sections of fixed brain, specifically the cerebral cortex, were stained with H&E (scale bars, 50 μm) (**a**) and antibodies against CD45 (scale bars, 100 μm) (**b**) perforin and CD45 (scale bars, 10 μm) (**f**). Nuclei are depicted by 4′,6-diamidino-2-phenylindole (DAPI) stain (blue). Single-cell suspensions of ZIKV-infected and mock *Ifnar1*$^{-/-}$ brains (n=6) were analyzed for quantification of CD45 positive cells by flow cytometry five (n=7) and seven days post infection (n=9) in three separate experiments. Data are presented as mean ± SD from an analysis of 1.5 million whole brain cells. (**c**). CD45+ cells were further analyzed for percentage of CD3+ and F4/80+ cells in 1.5 million whole brain cells (**d**) and quantification of CD4, CD8 through flow cytometry of isolated leukocytes from the brain (**e**). *P < 0.05; **P < 0.01 (two-tailed unpaired Student's t-test).

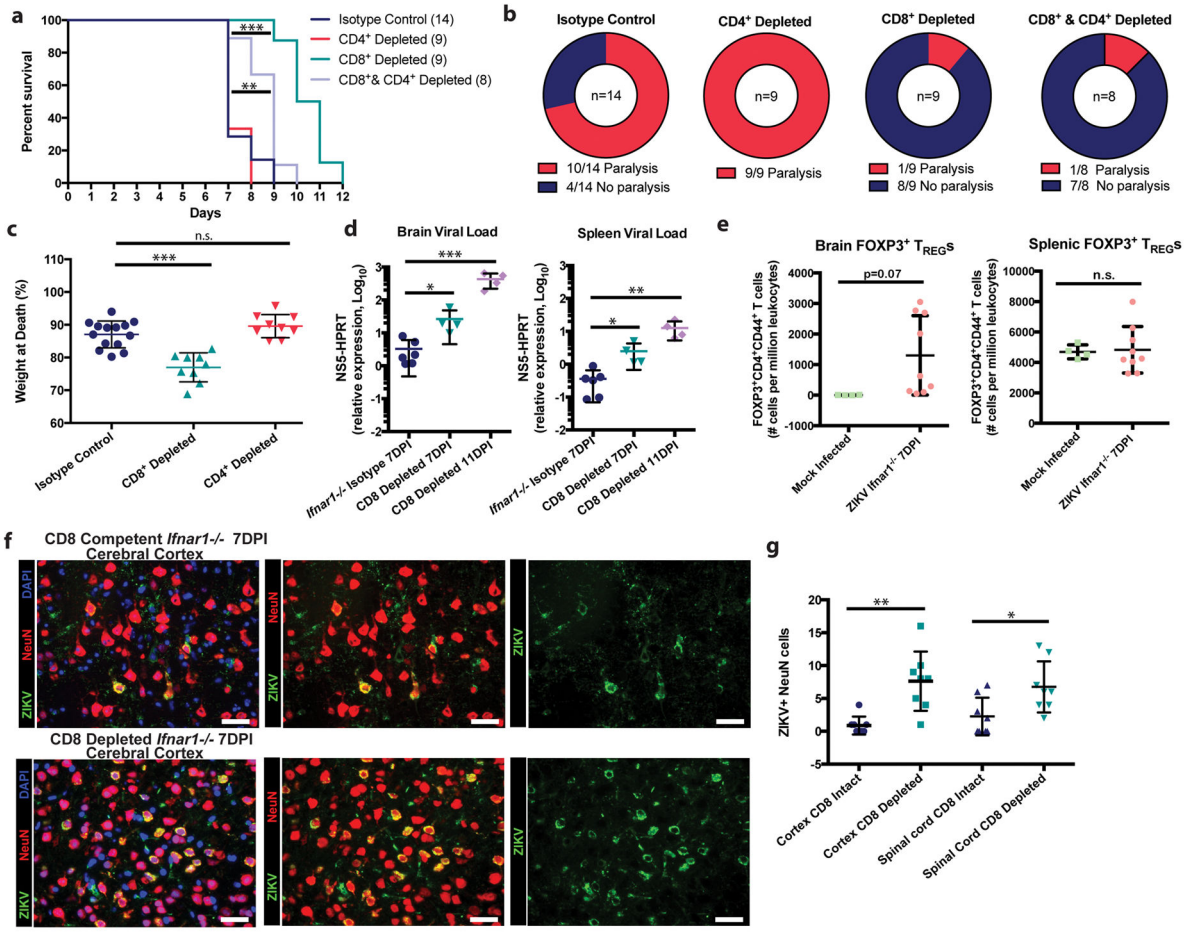

Figure 4. Antiviral activity of effector CD8$^+$ T cells within the brain limits ZIKV replication within neurons, but instigates ZIKV-associated paralysis

a–e, *Ifnar1*$^{-/-}$ were injected with depletion antibodies for CD8 (n=9), CD4 (n=9), CD4 and CD8 (n=8) or with isotype control (n=14) −1, 4 and 9 days post infection with 10^6 plaque-forming units (p.f.u.) of ZIKV intra-footpad in three separate experiments. Survival (**a**) development of hindlimb paralysis (**b**) were monitored with weight at time of sacrifice due to development of moribund state (onset of paralysis or >20% weight loss) was determined (**c**). **d**, Seven (and eleven for CD8 depleted) days post infection, viral load in tissue homogenates of brain and spleen were determined. Data are presented as mean ± SD (**d**). **e**, Intracellular Foxp3+ cells were analyzed via flow cytometry within ZIKV-infected (n=8) and mock (n=4) brains in two separate experiments. **f**, Frozen sections of the brain, specifically the cerebral cortex, seven days post infection were stained with antibodies against NeuN and ZIKV with nuclei are depicted by 4′,6-diamidino-2-phenylindole (DAPI) stain (blue) (scale bars, 50 μm). (**g**) ZIKV positive neurons within the cortex and distal spinal cord were quantified in CD8 intact and depleted murine tissues. *P < 0.05; **P < 0.01 ***P < 0.001 (two-tailed unpaired Student's t-test or log-rank test for survival curve).